

SVQ: Sparse Vector Quantization for Spatiotemporal Forecasting

Chao Chen*
Central South University
ccchaochen@csu.edu.cn

Hui Liu
Central South University
csulihui@csu.edu.cn

Tian Zhou*
Alibaba Group
tian.zt@alibaba-inc.com

Liang Sun
Alibaba Group
liang.sun@alibaba-inc.com

Yanjun Zhao
Alibaba Group
xiangyan.zyj@alibaba-inc.com

Rong Jin†
Meta Platform Inc
rongjinml@meta.com

Abstract

Spatiotemporal forecasting tasks, such as weather forecasting and traffic prediction, offer significant societal benefits. These tasks can be effectively approached as image forecasting problems using computer vision models. Vector quantization (VQ) is a well-known method for discrete representation that improves the latent space, leading to enhanced generalization and transfer learning capabilities. One of the main challenges in using VQ for spatiotemporal forecasting is how to balance between keeping enough details and removing noises from the original patterns for better generalization. We address this challenge by developing sparse vector quantization, or SVQ for short, that leverages sparse regression to make better trade-off between the two objectives. The main innovation of this work is to approximate sparse regression by a two-layer MLP and a randomly fixed or learnable matrix, dramatically improving its computational efficiency. Through experiments conducted on diverse datasets in multiple fields including weather forecasting, traffic flow prediction, and video forecasting, we unequivocally demonstrate that our proposed method consistently enhances the performance of base models and achieves state-of-the-art results across all benchmarks.

1. Introduction

Recent years have witnessed amazing progress in self-supervised learning, with well-known algorithms such as masked modeling [1] and contrastive learning [3]. However, existing self-supervised learning methods primarily focus on learning from static image data. Insufficient attention has been paid to spatiotemporal forecasting, which involves predicting future frames based on past frames. Research on spatiotemporal forecasting has significant applications in fields such as weather forecasting and traffic flow prediction. These tasks pose considerable challenges as they require the model to not only comprehend historical spatiotemporal

relationships, but also infer future dynamics with precise granularity both in temporal scale and spatial scale.

The existing spatiotemporal forecasting models are primarily recurrent-based, which are closely related to long short-term memory (LSTM), such as ConvLSTM [26], PredRNN [33], and E3D-LSTM [35]. Latest studies have shifted towards non-recurrent models [8, 27, 28], which offer higher prediction accuracy and computational efficiency.

In this work, we view spatiotemporal forecasting as an image prediction problem. One of the main challenges is how to balance two conflicting goals, i.e., prediction of future images in fine grained details and ensuring a good generalization of spatiotemporal forecasting by restricting the diversity of predicted patterns. To address this challenge, we propose sparse regression based vector quantization, or SVQ for short. Unlike typical vector quantization methods where a relatively small number of codes are used and each vector is assigned to one code, sparse regression uses a large number of codes and assigns each vector to multiple codes in order to cover diverse visual patterns without hurting the generalized performance. The main innovation of this work is to show that sparse regression, despite its complexity, can be well approximated by a two-layer MLP and a randomly fixed or learnable matrix, dramatically improving its computational efficiency. We emphasize that the proposed vector quantization method SVQ can be applied to any non-recurrent backbone to improve their prediction accuracy. Our experiments with multiple real-world benchmark datasets, including weather forecasting, traffic flow prediction, and video forecasting, clearly demonstrate the power of the proposed vector quantization method SVQ.

2. Related Work

2.1. Recurrent-based forecasting model

Most existing spatiotemporal forecasting models are based on spatial modeling techniques such as Conv2D [40], Conv3D [35], and Attention [19]. The main distinction among forecasting models is how they incorporate temporal information. Recurrent-based models, like ConvL-

* Equal contribution.

† The author completed the work while at Alibaba.

STM [26], have been widely used to capture motion dynamics by treating multi-frame prediction as an iterative process. Several modifications have been proposed to enhance the ConvLSTM structure. PredRNN [33] introduces the Spatiotemporal LSTM (ST-LSTM) unit to store spatial appearances and temporal variations in a single memory pool. PredRNN++ [34] and PredRNNV2 [37] further enhance the model depth and receptive field with cascade causal LSTM and a memory decoupling loss.

2.2. Non-recurrent forecasting model

Recurrent-based forecasting models are in general effective but at the price of higher computational cost due to their unparallelizable architectures. Some recent research of spatiotemporal forecasting has focused on non-recurrent models. They optimize the multi-frame forecasting objective without relying on autoregressive processes. SimVP [8, 27] divides learning into spatial and temporal components using an encoder-translator-decoder architecture, consistently outperforming recurrent-based models on video prediction benchmarks. TAU [28] builds on SimVP’s architecture by introducing a visual attention mechanism in the translator module. OpenSTL [29] enhances the translator module and proposes various MetaFormer models.

2.3. Vector quantization and sparse coding

Instead of using continuous latent, VQVAE [32] is a pioneer work that incorporates vector quantization to learn discrete latent representation. It typically assigns each vector to the closest code in the learned codebook. Many variants [7, 21, 22, 41, 42, 42, 45] have been proposed to further improve the representation power. Residual VQ [41, 45] recursively quantizes the residuals of input data. Finite scalar quantization (FSQ) [21] simplifies vector quantization in generative modeling by rounding each scalar value into discrete levels. Multi-headed VQ [22] adopts multiple codes for each vector (number of heads equals 8 in their paper).

Despite the effectiveness of above VQ-based methods, they still use a relatively small number of codes to represent the continuous vector. To circumvent this shortcoming, SCVAE [39] employs sparse coding and represents the vector by a sparse linear combinations of multiple codes. SCVAE adopts the widely used sparse coding algorithm to achieve end-to-end training, known as learnable iterative shrinkage thresholding algorithm (LISTA) [10]. The sparse coding method using LISTA is dubbed sparse vector quantization-raw (SVQ-raw) here. A significant drawback of SVQ-raw is its high computational complexity, which increases quadratically with the size of the codebook.

To the best of our knowledge, sparse vector quantization has not been applied to spatiotemporal forecasting yet. We hypothesize that sparse vector quantization ensures a good generalized performance for spatiotemporal forecasting.

3. Sparse Vector Quantization (SVQ)

In this section, we will first describe the mathematical foundation for SVQ, followed by the description of detailed implementation.

3.1. Vector quantization by sparse regression

Let $\{z_i \in \mathbb{R}^d\}_{i=1}^m$ be the set of codes. A typical vector quantization method assigns a data point $x \in \mathbb{R}^d$ to the nearest code in $\{z_i\}_{i=1}^m$. The main problem with such an approach is that a significant part of the information in x will be lost due to quantization. Sparse regression turns the code assignment problem into an optimization problem

$$w = \arg \min_{w \in \mathbb{R}_+^m} \frac{1}{2} \left\| x - \sum_{i=1}^m w_i z_i \right\|^2 + \lambda |w|_1, \quad (1)$$

where $w = (w_1, \dots, w_m) \in \mathbb{R}_+^m$ is the weight for combining codes $\{z_i\}_{i=1}^m$ to approximate x . By introducing L_1 regularizer in the optimization problem, we effectively enforce x to be associated with a small number of codes. Compared to classic VQ methods where codes have to be learned through clustering, according to [4], it is sufficient to use randomly sampled vectors as codes as long as its number is large enough, thus avoiding the need of computing and adjusting codes. The theoretical guarantee of sparse regression is closely related to the property of subspace clustering, as revealed in *Theorem 1*.

As shown in Figure 1, the obvious downside of sparse regression for VQ is its high computational cost, as it needs to solve the optimization problem in (1) for EVERY data point. Below, we will show that sparse regression can be approximated by a two-layer MLP and a randomly fixed or learnable matrix, making it computationally attractive.

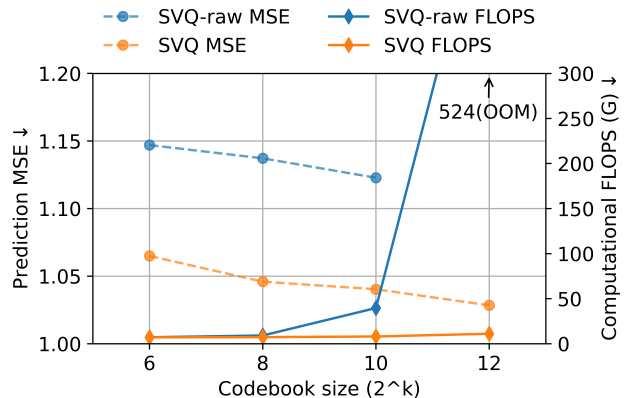


Figure 1. Computational efficiency (FLOPS) and prediction error (MSE) on WeatherBench-S temperature dataset with SVQ-raw and SVQ. The computational complexity of SVQ-raw increases quadratically with the size of codebook, making it suffer from out-of-memory (OOM) issue when scaling codebook size up to 2^{12} .

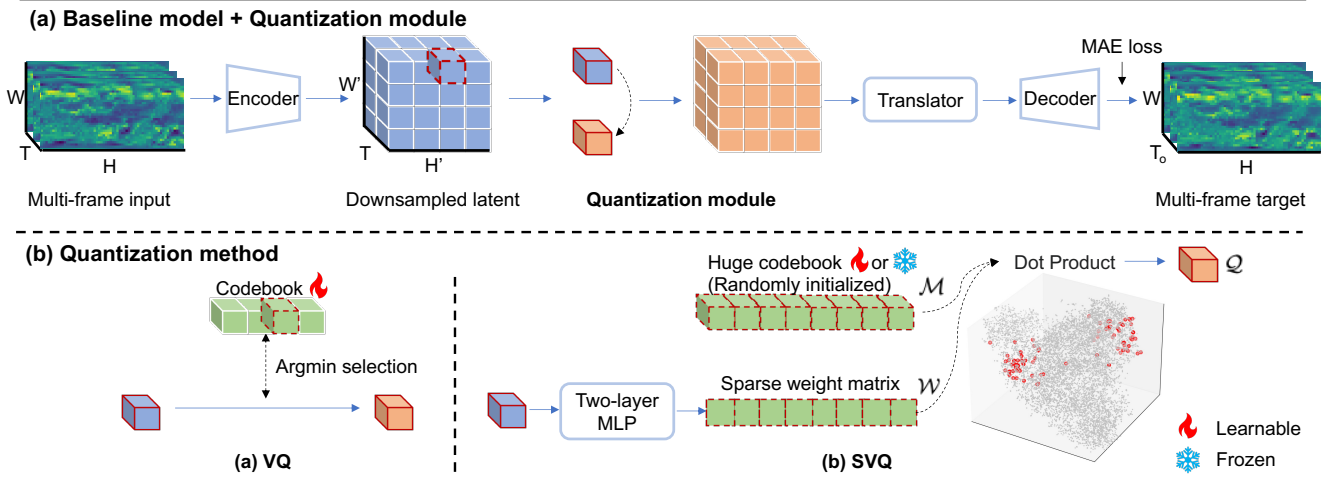


Figure 2. (a) Overall framework of baseline model and the proposed quantization module. The encoder, translator, decoder are inherited from SimVP to extract spatial features, learn temporal dependencies, and reconstruct prediction frames, respectively. A quantization module is added between the encoder and translation to effectively ensure a good generalized performance. (b) Visualization of the classic VQ and our proposed SVQ method. In contrast, SVQ select multiple codes (red dots) from a huge codebook (grey dots), and the codebook can be either learnable or frozen.

To solve the optimization problem (1), we consider the composite optimization method whose iteration is given as follows

$$w'_{t+1} = w_t - \eta Z^\top (Z w_t - x), \quad w_{t+1} = [w'_{t+1} - \lambda \eta \mathbf{1}]_+,$$

where $Z = (z_1, \dots, z_m)$ and $[a]_+$ outputs 0 if $a < 0$ and a otherwise. We consider the first step of the iteration where $w_0 = 0$ and have $w = \eta [Z^\top x - \lambda \mathbf{1}]_+ = \eta \sigma (Z^\top x - \lambda)$ and the resulting output for x is given as

$$x' = \sum_{i=1}^m w_i z_i = \eta Z \sigma (Z^\top x - \lambda).$$

By generalizing ηZ into another matrix B , we have output vector x' exactly expressed as a matrix and a two-layer MLP over x . We finally note that although it is convenient to form the codebook by randomly sampling vectors, we found empirically that tuning codebook does bring slight additional gains.

3.2. Detailed implementation

Architecture of baseline model. As shown in Figure 2, we adopt SimVP [8] as our baseline model and add the quantization module between the encoder and translator. Formally, the input data of SVQ is a 4D tensor $X \in \mathbb{R}^{H \times W \times T \times C}$, where H, W, T, C denote height, width, time steps, channels, respectively. It first goes through an encoder En to get downsampled latent representation $\text{En}(X) \in \mathbb{R}^{H' \times W' \times T \times C'}$, where H', W', C' denote the height, width, and channels of latent representation. Since encoder and decoder only process the spatial dependencies, the dimension of time

steps remains consistent. The latent representation comprises $H' \times W' \times T$ tokens, where each token is a vector with length of C' . Quantization module replaces every token vector with corresponding discrete values in codebook. To encourage sparsity in the intermediate weight matrix, we incorporate a Mean Absolute Error (MAE) loss to the output as a surrogate form of regularization.

Quantization module. SVQ comprises a two-layer MLP and a huge codebook. The codebook is a randomly initialized matrix $\mathcal{M} \in \mathbb{R}^{N \times C'}$, where N denotes the size of codebook. To achieve automatic selection of codes, we generate a weight matrix $\mathcal{W} \in \mathbb{R}^{H' \times W' \times T \times N}$ by nonlinear projection from latent representation $\text{En}(X)$, which can be formally expressed as:

$$\mathcal{W} = \text{MLP}(\text{En}(X)). \quad (2)$$

where the MLP contains two linear layers and an intermediate ReLU activation.

Then, the quantized output Q is the dot product of weight matrix and codebook matrix, which can be considered as a selection process (Figure 2):

$$Q = \mathcal{W} \cdot \mathcal{M}, \quad (3)$$

4. Efficient Utilize of Cookbook Using Sparse Regression

To understand the difference between sparse regression based quantization scheme and clustering based quantization scheme, we measure the number of codes that we need in order to approximate any vector within an unit ball \mathcal{B} with error less than δ . We denote this number by $T(\mathcal{B}, \delta)$. As indicated by the theorem below, using sparse regression, $T(\mathcal{B}, \delta)$

can be reduced from $O(1/\delta^d)$ to $O(1/\delta^p)$, with $p \ll d$ for high dimensional vectors.

Theorem 1. $T(\mathcal{B}, \delta)$ for the clustering based method is at least $1/\delta^d$, while $T(\mathcal{B}, \delta)$ for sparse regression can be $(4d/\delta)^p$, with

$$p \geq \max\left(3, \frac{\log(4/\delta)}{\log \log(2d/\varepsilon)}\right),$$

as long as the non-zero elements used by sparse regression is at least $\frac{4d}{\delta(\log C + p \log(4d) - (p+1) \log \delta)}$.

Proof. To bound $T(\mathcal{B}, \delta)$ for the clustering method, we directly use the covering number result for an unit ball, i.e. in order to approximate any vector in a unit ball \mathcal{B} within an error δ , you need at least $1/\delta^d$ code vectors. To bound $T(\mathcal{B}, \delta)$, we consider Ug , where $U = (u_1, \dots, u_m)$ includes randomly sampled vectors, with each u_k sampled from $\mathcal{N}(0, I_d/m)$ and $g \in \Delta_s$ is an unit vector with s non-zero elements. Since

$$\Pr(|UU^\top - I|_2 \geq \gamma) \leq 2d \exp\left(-\frac{m\gamma^2}{3d}\right),$$

we have, with a probability $1 - \varepsilon$,

$$|UU^\top - I|_2 \leq \Delta := \sqrt{\frac{d}{m} \log \frac{2d}{\varepsilon}}.$$

Thus, with a probability $1 - \varepsilon$, we have for any g and g'

$$|g' - g|_2 \geq \frac{1}{1 + \Delta} |Ug - Ug'|.$$

Since the covering number for s -sparse unit vector is upper bounded by $(Cm/s\delta)^s$, using the fact that packing number upper bounds the covering number, we know that to approximate any vector in the unit ball \mathcal{B} , we need

$$\left(\frac{Cm}{s\delta}\right)^s \geq \left(1 + \frac{2}{\delta}\right)^d (1 + \Delta)^d.$$

By choosing $m = (4d/\delta)^p$, we have

$$(1 + \Delta)^d \leq \exp(d\Delta) \leq e$$

and therefore

$$\left(\frac{C'm}{s\delta}\right)^s \geq \left(1 + \frac{2}{\delta}\right)^d,$$

where $C' = Ce$. It leads to

$$s \log \frac{C'm}{\delta} \geq \frac{2d}{\delta} + s \log s.$$

Since

$$s \geq \frac{4d}{\delta(\log C + p \log(4d) - (p+1) \log \delta)}$$

it is easy to verify that $s \log s \leq 2d/\delta$, leading to

$$m \geq \left(\frac{4d}{\delta}\right)^p.$$

5. Experiments

In this section, we extensively evaluate SVQ on a wide range of real-world spatiotemporal forecasting datasets. The experiments are conducted to investigate our model from different perspectives:

- Boosting performance of various backbones. SVQ serves as a versatile plug-in module applicable to various types of MetaFormers [43].
- Forecasting performance compared with state-of-the-art (SOTA) models.
- Importance of each design decision. We conduct a series of ablation studies to verify the effectiveness of our framework design.

Besides, we perform a comprehensive comparative analysis between SVQ and classic VQ methods. Due to page limit, please refer to the supplementary material for more information.

Dataset. Weather forecasting and traffic-related prediction are critical tasks in spatiotemporal forecasting. We first evaluate our algorithm on two benchmark datasets, i.e., WeatherBench [24] and TaxiBJ [46]. Additionally, we evaluate the generalization ability on three well-known video forecasting tasks, including human pose (Human3.6M [14]), driving scene (KittiCaltech [5, 9]), and human action (KTH Action [25]). Table 1 summarizes the dataset statistics.

Table 1. The detailed statistics of benchmark datasets.

Dataset	Size		Seq. Len.		Img. Shape H × W × C	Interval
	train	test	in	out		
WeatherBench-S	2,167	706	12	12	32 × 64 × 1	1 hour
WeatherBench-M	54,019	2,883	4	4	32 × 64 × 4	6 hour
TaxiBJ	20,461	500	4	4	32 × 32 × 2	30 min
KittiCaltech	3,160	3,095	10	1	128 × 160 × 3	Frame
Human3.6M	73,404	8,582	4	4	256 × 256 × 3	Frame
KTH Action	4,940	3,030	10	20	128 × 128 × 1	Frame

Experimental details. We follow the training setting and hyperparameters of OpenSTL [29]. The best MetaFormer for each dataset is selected based on OpenSTL benchmark results. For SVQ, we set the codebook size to 10000 for WeatherBench, TaxiBJ, and Human3.6M, and 6000 for KittiCaltech and KTH. The hidden dimension of non-linear projection layer is fixed at 128. We conduct experiments on 1 or 4 NVIDIA V100 32GB GPUs with a total batch size of 16. More details of architecture and hyperparameters can be found in the supplementary material.

Metrics. We evaluate the forecasting error on the mean squared error (MSE) and mean absolute error (MAE). We assess the image quality of the predicted frames using structural similarity index measure (SSIM) [38], peak signal-to-noise ratio (PSNR), and learned perceptual image patch similarity (LPIPS) [47]. The training process is early stopped with a patience of 10, and the models with the lowest loss are saved for further evaluation.

5.1. Sparse vector quantization boosting performance

To assess the universality of SVQ, we utilize diverse MetaFormers [43] as backbones to substitute the translator module, following prior work [29]. Our selection of MetaFormers comprises CNN-based, Transformer-based, and MLP-based: Swin Transformer [17], ViT [6], Poolformer [44], Uniformer [15], IncepU [8], gSTA [27], VAN [12], MogaNet [16], HorNet [23], and MLP-Mixer [30]. We conduct experiments on WeatherBench-S temperature dataset because it is lightweight and fast for training.

Table 2. Boosting performance of SVQ for various MetaFormers on WeatherBench-S temperature dataset.

MetaFormer	MSE		MAE	
	w/o SVQ	w SVQ	w/o SVQ	w SVQ
IncepU[8]	1.238	1.216	0.7037	0.6831
gSTA[27]	1.131	1.018	0.6633	0.6109
ViT[6]	1.146	1.111	0.6712	0.6375
Swin[17]	1.143	1.088	0.6735	0.6320
Uniformer[15]	1.204	1.110	0.6885	0.6400
MLP-Mixer[30]	1.255	1.120	0.7011	0.6455
ConvMixer[31]	1.267	1.257	0.7073	0.6780
Poolformer[44]	1.156	1.097	0.6715	0.6297
ConvNeXt[18]	1.277	1.159	0.7220	0.6568
VAN[12]	1.150	1.083	0.6803	0.6342
HorNet[23]	1.201	1.130	0.6906	0.6472
MogaNet[16]	1.152	1.067	0.6665	0.6271
Average improvement	↑ 4.9%		↑ 6.0%	

As shown in Table 2, our framework consistently improves the performance across all MetaFormers, showcasing its universality and effectiveness across different types of backbones. The average reduction of MSE and MAE reaches **4.9%** and **6.0%**, respectively. The gSTA is the best backbone, while our SVQ further improves its performance by 10.0%. This outcome also aligns with our motivation that the noisy learning process is persuasive in spatiotemporal forecasting, irrespective of the model design. By adopting SVQ to restrict the predicted patterns and ensure a good generalized performance, researchers can concentrate on designing high-quality and general base models.

5.2. Forecasting performance on various tasks

We use SimVP with the best MetaFormer as backbone and integrate our SVQ module. Both frozen and learnable SVQ are applied. Their forecasting performance is compared with baselines under the unified framework of OpenSTL. The baselines consist of two categories: 1) Non-recurrent models like SimVP [8] and TAU [28]; 2) Recurrent-based models like ConvLSTM [26], PredNet [20], PredRNN [33], PredRNN++ [34], MIM [36], E3D-LSTM [35], PhyDNet [11], MAU [2], PredRNNv2 [37], and DMVFN [13]. We copy all baseline results from the original OpenSTL paper. Notably, SVQ achieves either the best or comparable performance across all datasets. Interestingly, we find that when codebook size is large, the performance of frozen randomly-initialized codebook is on par with carefully learned codebook.

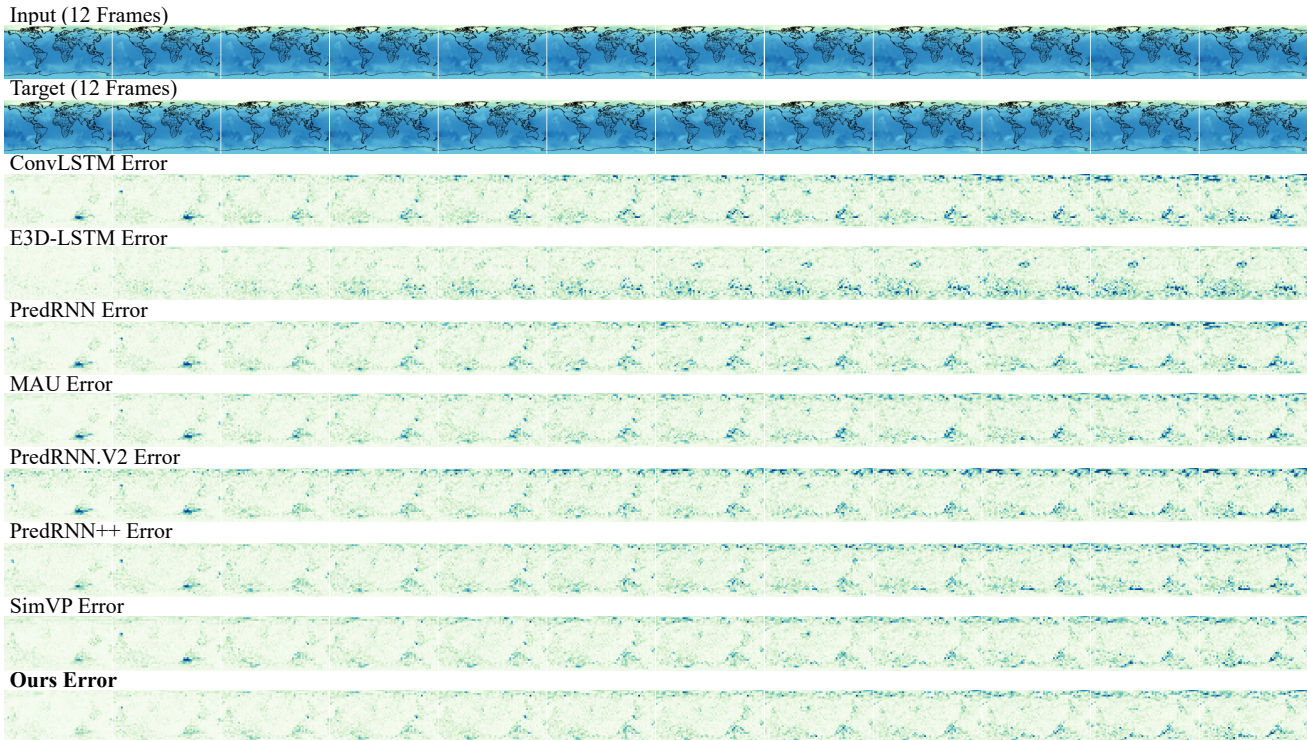


Figure 3. The qualitative forecasting results on WeatherBench-S temperature dataset.

Table 3. Performance comparison for SVQ module and baseline models on WeatherBench. WeatherBench-S is single-variable, one-hour interval forecasting setup trained on data from 2010-2015, validated on 2016, and tested on 2017-2018. WeatherBench-M targets broader application, which is multi-variable, six-hour interval forecasting setup trained on data from 1979-2015, validated on 2016, and tested on 2017-2018. The top two results are highlighted by bold or underlined.

Dataset	Variable	Temperature		Humidity		Wind Component		Total Cloud Cover	
	Model	MSE↓	MAE↓	MSE↓	MAE↓	MSE↓	MAE↓	MSE↓	MAE↓
WeatherBench-S	ConvLSTM[26]	1.521	0.7949	35.146	4.012	1.8976	0.9215	0.0494	0.1542
	E3D-LSTM[35]	1.592	0.8059	36.534	4.100	2.4111	1.0342	0.0573	0.1529
	PredRNN[33]	1.331	0.7246	37.611	4.096	1.8810	0.9068	0.0550	0.1588
	MIM[36]	1.784	0.8716	36.534	4.100	3.1399	1.1837	0.0573	0.1529
	MAU[2]	1.251	0.7036	34.529	4.004	1.9001	0.9194	0.0496	0.1516
	PredRNN++[34]	1.634	0.7883	35.146	4.012	1.8727	0.9019	0.0547	0.1543
	PredRNN.V2[37]	1.545	0.7986	36.508	4.087	2.0072	0.9413	0.0505	0.1587
	TAU[28]	1.162	0.6707	31.831	3.818	1.5925	0.8426	0.0472	<u>0.1460</u>
	SimVP (w/o VQ)[8]	1.131	0.6633	31.750	3.818	1.5075	0.8178	0.0465	0.1471
	SimVP+SVQ (Frozen)	<u>1.023</u>	<u>0.6131</u>	<u>30.863</u>	<u>3.661</u>	<u>1.4337</u>	<u>0.7861</u>	0.0456	0.1456
	SimVP+SVQ (Learnable)	1.018	0.6109	30.611	3.657	1.4186	0.7858	<u>0.0458</u>	0.1463
WeatherBench-M	Variable	Temperature		Humidity		Wind U Component		Wind V Component	
	ConvLSTM[26]	6.303	1.7695	368.15	13.490	30.002	3.8923	30.789	3.8238
	PredRNN[33]	5.596	1.6411	354.57	13.169	27.484	3.6776	28.973	3.6617
	MIM[36]	7.515	1.9650	408.24	14.658	35.586	4.2842	36.464	4.2066
	MAU[2]	5.628	1.6810	363.36	13.503	27.582	3.7409	27.929	3.6700
	PredRNN++[34]	5.647	1.6433	363.15	13.246	28.396	3.7322	29.872	3.7067
	PredRNN.V2[37]	6.307	1.7770	368.52	13.594	29.833	3.8870	31.119	3.8406
	TAU[28]	4.904	1.5341	<u>342.63</u>	12.801	24.719	3.5060	25.456	3.4723
	SimVP (w/o VQ)[8]	4.833	1.5246	340.06	12.738	24.535	3.4882	25.232	3.4509
	SimVP+SVQ (Frozen)	4.427	1.4160	360.15	12.445	<u>23.915</u>	<u>3.4078</u>	24.968	<u>3.4117</u>
	SimVP+SVQ (Learnable)	<u>4.433</u>	<u>1.4164</u>	360.53	<u>12.449</u>	23.908	3.4060	<u>24.983</u>	3.4095

WeatherBench and TaxiBJ. Weather forecasting and traffic flow prediction are two macro forecasting tasks. These two datasets are collected at low frequencies (30min or 1-6h) and exhibit stable states, which is especially challenging for the model to capture subtle changes. The qualitative and quantitative results of WeatherBench are reported in Figure 3 and Table 3. The qualitative and quantitative results of TaxiBJ are reported in Figure 4 and Table 4.

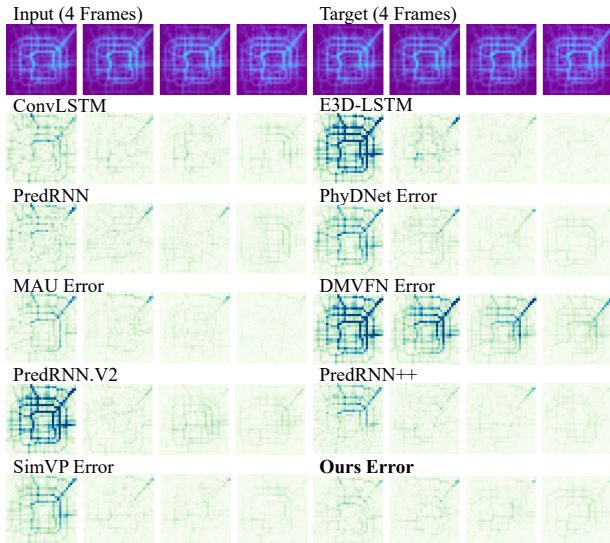


Figure 4. The qualitative forecasting results on TaxiBJ dataset.

Table 4. Performance comparison for SVQ and baseline models on TaxiBJ. The top two results are highlighted by bold or underlined.

Model	MSE↓	MAE↓	SSIM↑	PSNR↑
ConvLSTM[26]	0.3358	15.32	0.9836	39.45
E3D-LSTM[35]	0.3427	14.98	0.9842	39.64
PhyDNet[11]	0.3622	15.53	0.9828	39.46
PredNet[20]	0.3516	15.91	0.9828	39.29
PredRNN[33]	0.3194	15.31	0.9838	39.51
MIM[36]	<u>0.3110</u>	14.96	0.9847	39.65
MAU[2]	0.3268	15.26	0.9834	39.52
DMVFN[13]	3.3954	45.52	0.8321	31.14
PredRNN++[34]	0.3348	15.37	0.9834	39.47
PredRNN.V2[37]	0.3834	15.55	0.9826	39.49
TAU[28]	0.3108	14.93	0.9848	39.74
SimVP (w/o VQ)[8]	0.3246	15.03	0.9844	39.71
SimVP+SVQ (Frozen)	0.3171	<u>14.68</u>	<u>0.9848</u>	<u>39.83</u>
SimVP+SVQ (Learnable)	0.3191	14.64	0.9849	39.86
Improvement	↑1.7%	↑2.6%	↑0.1%	↑0.4%

WeatherBench has significant differences between various terrains. Non-recurrent models like SimVP and TAU excel at spatial learning and generally outperform the other baselines. Our SVQ module helps to learn robust representation for noisy data and further improves SimVP across all metrics and variables. On the WeatherBench-S temperature dataset, SVQ significantly outperforms the best baseline by **10.0%** (1.131 → 1.018). SimVP provides a strong baseline on TaxiBJ. Our SVQ module still consistently enhances its performance and effectively reduces the forecasting errors in the central spots of the predicted frames.

Table 5. Performance comparison for SVQ and baseline models on Human3.6M, KTH, and KittiCaltech. The top two results are highlighted by bold or underlined.

Dataset	Human3.6M				KittiCaltech				KTH			
	MAE↓	SSIM↑	PSNR↑	LPIPS↓	MAE↓	SSIM↑	PSNR↑	LPIPS↓	MAE↓	SSIM↑	PSNR↑	LPIPS↓
ConvLSTM[26]	1583.3	0.9813	33.40	0.03557	1583.3	0.9345	27.46	0.08575	445.5	0.8977	26.99	0.26686
E3D-LSTM[35]	1442.5	0.9803	32.52	0.04133	1946.2	0.9047	25.45	0.12602	892.7	0.8153	21.78	0.48358
PredNet[20]	1625.3	0.9786	31.76	0.03264	1568.9	0.9286	27.21	0.11289	783.1	0.8094	22.45	0.32159
PhyDNet[11]	1614.7	0.9804	39.84	0.03709	2754.8	0.8615	23.26	0.32194	765.6	0.8322	23.41	0.50155
MAU[2]	1577.0	0.9812	33.33	0.03561	1800.4	0.9176	26.14	0.09673	471.2	0.8945	26.73	0.25442
MIM[36]	1467.1	0.9829	33.97	0.03338	1464.0	0.9409	28.10	0.06353	380.8	0.9025	27.78	0.18808
PredRNN[33]	1458.3	0.9831	33.94	0.03245	1525.5	0.9374	27.81	0.07395	380.6	0.9097	27.95	0.21892
PredRNN++[34]	1452.2	0.9832	34.02	0.03196	1453.2	0.9433	28.02	0.13210	370.4	0.9124	28.13	<u>0.19871</u>
PredRNN.V2[37]	1484.7	0.9827	33.84	0.03334	1610.5	0.9330	27.12	0.08920	368.8	0.9099	<u>28.01</u>	0.21478
TAU[28]	1390.7	<u>0.9839</u>	34.03	0.02783	1507.8	0.9456	27.83	<u>0.05494</u>	421.7	0.9086	27.10	0.22856
SimVP (w/o VQ)[8]	1441.0	0.9834	<u>34.08</u>	0.03224	1507.7	0.9453	27.89	0.05740	397.1	0.9065	27.46	0.26496
SimVP+SVQ (Frozen)	1264.9	0.9851	34.07	<u>0.02380</u>	1408.6	0.9469	28.10	0.05535	<u>364.6</u>	0.9109	27.28	0.20988
SimVP+SVQ (Learnable)	<u>1265.1</u>	0.9851	34.06	0.02367	<u>1414.9</u>	0.9458	28.10	0.05776	360.2	<u>0.9116</u>	27.37	0.20658
Improvement	↑12.2%	↑0.2%	↓0.0%	↑26.2%	↑6.6%	↑0.2%	↑0.8%	↑3.6%	↑9.3%	↑0.6%	↓0.3%	↑22.0%

Human3.6M, KittiCaltech and KTH. To test SVQ on general cases, we further conduct experiments on popular video prediction tasks. Due to the diversity and complexity of real-world videos, these datasets have severe temporal distribution shift. The quantitative results are reported in Table 5. Human3.6M dataset showcases delicate variations between consecutive frames, which exhibits a low-frequency signal. KittiCaltech dataset is especially challenging due to fast, dynamic backgrounds and limited training data. KTH dataset evaluates the ability of long-horizon predictions (predict 20 future frames given 10 past frames). As for the baselines, SimVP achieves competitive performance on Human3.6M and KittiCaltech, while recurrent-based models like PredRNN++ prevail on KTH due to strong temporal modeling capabilities. Despite the difference among these tasks, SVQ consistently improves the SimVP model across all datasets. It not only brings lower forecasting errors (average **9.4%** reduction in MAE), but also significantly improves image quality (average **17.3%** reduction in LPIPS). Notably, PredRNN++ and MIM are the best baselines on KittiCaltech. However, even without recurrent design, our SimVP-SVQ model outperforms them across all metrics.

5.3. Ablation study

We conduct a series of ablation studies on WeatherBench-S temperature dataset to understand the contribution of important designs based on the default setting: SVQ with 10000 codebook size, learnable codebook, and MAE loss.

Vector quantization method. To comprehensively compare the discrete representation methods in spatiotemporal forecasting task, we apply a series of well-known VQ methods, including VQ [32], residual VQ [45], grouped residual VQ [41], multi-headed VQ [22], residual finite scalar quantization (FSQ) [21], lookup free quantization (LFQ) [42], and residual LFQ [42]. To make a fair comparison, the VQ methods are applied following the same approach as SVQ, which acts as a plug-in module and trained along with back-

bone model. We reproduce the results using the source code provided on the GitHub page. As shown in Table 6, SVQ directly improves the spatiotemporal forecasting performance as an efficient plug-in, while the other quantization methods degrade forecasting performance. This result aligns with Section 4 that SVQ has better representation power than clustering based quantization methods. The other VQ methods require massive training data and a complicated, parameter-consuming model to further build the prior distribution of codes, such as an autoregressive transformer in VQGAN [7] or a BERT-style masked transformer in MaskGIT [1]. We do not intend to imply that our SVQ can beat the other VQ methods on general image generation tasks. Instead, we highlight that SVQ is efficient and brings direct improvement on common real-world spatiotemporal forecasting tasks.

Table 6. Ablation of vector quantization method.

Method	MSE↓	MAE↓
VQ[32]	1.8544	0.8963
Residual VQ[45]	1.8882	0.9237
Grouped Residual VQ[41]	1.1737	0.6747
Multi-headed VQ[22]	1.2113	0.6994
Residual Finite Scalar Quantization[21]	1.3192	0.7505
Lookup Free Quantization (LFQ)[42]	2.9875	1.1103
Residual LFQ[42]	1.2806	0.7281
SVQ-raw[39]	1.1228	0.6456
SVQ	1.0182	0.6109

Codebook size and learnability. We compare the effect of codebook size when codebook is learnable or frozen (Table 7). We find that increasing codebook size gradually improves performance. When significantly increasing codebook size to a large value (such as 10000), difference between frozen and learnable codebook narrows, which is 0.5% (1.0230 → 1.0182) in this case. We hypothesize that when we increase the size of codebook significantly, we do not need to carefully learn codes in codebook, making com-

<https://github.com/lucidrains/vector-quantize-pytorch/tree/master>

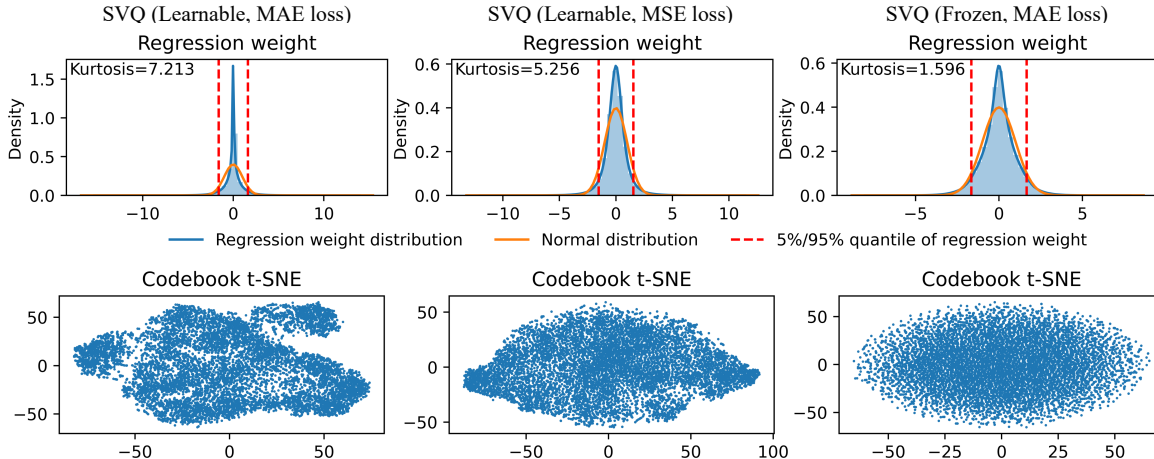


Figure 5. Distribution of regression weight \mathcal{W} and codebook \mathcal{M} . Higher kurtosis represents more compact and concentrate distribution near zero, as well as sparser regression weights. Learnable codebook and MAE loss encourage sparser weights and a more structured codebook.

bination of randomly initialized code is almost as good as any carefully learned results. Furthermore, the SVQ structure that we designed outperforms the one-layer variant and the bucket-shape variant, despite having similar numbers of parameters.

Table 7. Ablation of codebook size and learnability.

Learnability	Projection dim	Codebook size	MSE↓	MAE↓
Frozen	128	10	1.0696	0.6227
	128	1000	1.0436	0.6198
	128	10000	1.0230	0.6131
Learnable	128	10	1.0492	0.6200
	128	1000	1.0479	0.6182
	128	10000	1.0182	0.6109
	1280(Bucket-shape)	1280	1.0352	0.6149
	None(One-layer)	10000	1.0425	0.6144

Self-learned sparse regression structure. The original SimVP model adopt MSE as prediction loss. We individually replace it with MAE loss and add the SVQ module, and find that the joint use of SVQ and MAE loss is necessary and brings significant improvement (Table 8). We hypothesize that the sparsity of weight matrix \mathcal{W} can benefit the representation learning of vector. To quantitatively evaluate the sparsity, we first transform the weight matrix \mathcal{W} to a normalized vector and then estimate the kurtosis of its distribution. As shown in Figure 5, we find that both learnable codebook and MAE loss encourage sparser weights. To further understand the behaviour of sparsity, we compare four types of codebook initialization methods under learnable or frozen cases (Table 9). We find that learnable codebook triggers sparser regression across different codebook initialization methods, which empirically proves that: 1) sparse regression is a self-learned structure, and 2) MAE loss can propagate and regularize the intermediate representation learning even when applied to the output.

Table 8. Module ablation.

Module	MSE↓	MAE↓
SimVP (MSE loss)	1.1308	0.6633
SimVP (MAE loss)	1.1265	0.6509
SimVP+SVQ (Learnable, MSE loss)	1.0994	0.6527
SimVP+SVQ (Learnable, MAE loss)	1.0182	0.6109

Table 9. Ablation of codebook initialization method.

Learnability	Initialization	MSE↓	MAE↓	Kurtosis
Frozen	kaiming uniform	1.0230	0.6131	1.596
	sparse(sparsity=0.9)	1.0498	0.6183	4.165
	trunc normal	1.0497	0.6166	1.582
	orthogonal	1.0343	0.6170	1.561
Learnable	kaiming uniform	1.0182	0.6109	7.213
	sparse(sparsity=0.9)	1.0342	0.6160	41.558
	trunc normal	1.0307	0.6161	4.236
	orthogonal	1.0302	0.6131	35.774

6. Conclusions

This paper introduces SVQ, an exceptionally straightforward yet highly effective plug-in module for sparse vector quantization in spatiotemporal forecasting tasks. By leveraging a two-layer MLP and a randomly fixed or learnable matrix to approximate sparse regression, SVQ offers a simple and efficient solution that can be easily integrated into various backbones, resulting in a significant boost in performance. Through rigorous experimentation across diverse datasets in weather forecasting, traffic flow prediction, and video forecasting, our proposed method consistently achieves state-of-the-art performance across all benchmark measures. We believe that this plug-in serves as a cost-effective and powerful alternative to traditional VQ methods for general spatiotemporal forecasting tasks.

SVQ: Sparse Vector Quantization for Spatiotemporal Forecasting

Supplemental Materials

The supplementary material for our work *SVQ: Sparse Vector Quantization for Spatiotemporal Forecasting* is organized as follows: Section **A** provides architectures and hyperparameters of SimVP model and VQ methods. Section **B** summarizes the computational cost of all forecasting models. Additional experiments on comparison of VQ methods, position of quantization module, and ablation of frozen module are then presented in Section **C**. Finally, Section **D** shows additional qualitative results of forecasting samples, and the effect of SVQ on latent representation.

A. Implementation details

A.1. Architecture configuration of SimVP

Table 10 reports the architectures of SimVP on all datasets. We select the best translator (or MetaFormer) based on OpenSTL benchmarks. The parameters remain unchanged, following the original configurations.

Table 10. Detailed configuration of SimVP backbone.

Dataset	Translator	spatio_kernel	hid_S	hid_T	N_T	N_S	drop_path	LR scheduler
WeatherBench-S temperature	gSTA	enc=3, dec=3	32	256	8	2	0.1	cosine
WeatherBench-S humidity	Swin	enc=3, dec=3	32	256	8	2	0.2	cosine
WeatherBench-S wind component	Swin	enc=3, dec=3	32	256	8	2	0.2	cosine
WeatherBench-S total cloud cover	gSTA	enc=3, dec=3	32	256	8	2	0.1	cosine
WeatherBench-M	MogaNet	enc=3, dec=3	32	256	8	2	0.1	cosine
TaxiBJ	ConvNeXt	enc=3, dec=3	32	256	8	2	0.1	cosine
Human3.6M	gSTA	enc=3, dec=3	64	512	6	4	0.1	cosine
KTH	IncepU	enc=3, dec=3	64	256	6	2	0.1	onecycle
KittiCaltech	gSTA	enc=3, dec=3	64	256	6	2	0.2	onecycle

A.2. Parameters of compared VQ methods

Table 11 reports the parameters of compared VQ methods corresponding to Table 6. The parameters are kept the same as the recommended setting on the GitHub repository to ensure their performance. To ensure a fair comparison, we also conduct an additional experiment for VQ methods using the same codebook size in Section C.1.

Table 11. Parameters of the compared VQ methods.

Vector quantization method	codebook_size	num_quantizers	groups	heads	Specific parameters
VQ	512	-	-	-	-
Residual VQ	1024	8	-	-	shared_codebook=True, stochastic_sample_codes=True
Grouped Residual VQ	1024	8	2	-	-
Multi-headed VQ	1024	-	-	8	separate_codebook_per_head=False
Residual Finite Scalar Quantization	-	8	-	-	levels=[8, 5, 5, 3]
Lookup Free Quantization (LFQ)	8192	-	-	-	entropy_loss_weight=0.1
Residual LFQ	256	8	-	-	-

B. Computational cost

Table 12 presents the computational costs of SVQ module and state-of-the-art forecasting models. It shows that recurrent-based models have significantly higher FLOPS requirements, while non-recurrent models are more efficient. The proposed SVQ module is not only effective but also computationally cheap. Across all datasets, SVQ only slightly increases the number of parameters and FLOPS. The computational burden of SimVP+SVQ is still significantly smaller than recurrent-based models.

https://openstl.readthedocs.io/en/latest/model_zoos/video_benchmarks.html
https://openstl.readthedocs.io/en/latest/model_zoos/weather_benchmarks.html
https://openstl.readthedocs.io/en/latest/model_zoos/traffic_benchmarks.html
<https://github.com/lucidrains/vector-quantize-pytorch/tree/master>

Table 12. Number of parameters and computing performance for all forecasting models.

Model type	Dataset	Human3.6M		KTH		KittiCaltech		WeatherBench-S		TaxiBJ	
	Model	Params	FLOPS	Params	FLOPS	Params	FLOPS	Params	FLOPS	Params	FLOPS
Recurrent-based	ConvLSTM	15.5M	347.0G	14.9M	1368.0G	15.0M	595.0G	14.98M	136G	14.98M	20.74G
	E3D-LSTM	60.9M	542.0G	53.5M	217.0G	54.9M	1004G	51.09M	169G	50.99M	98.19G
	PredNet	12.5M	13.7G	12.5M	3.4G	12.5M	12.5M	-	-	12.5M	0.85G
	PhyDNet	4.2M	19.1G	3.1M	93.6G	3.1M	40.4G	3.09M	36.8G	3.09M	5.60G
	MAU	20.2M	105.0G	20.1M	399.0G	24.3M	172.0G	5.46M	39.6G	4.41M	6.02G
	MIM	47.6M	1051.0G	39.8M	1099.0G	49.2M	1858G	37.75M	109G	37.86M	64.10G
	PredRNN	24.6M	704.0G	23.6M	2800.0G	23.7M	1216G	23.57M	278G	23.66M	42.40G
	PredRNN++	39.3M	1033.0G	38.3M	4162.0G	38.5M	1803G	38.31M	413G	38.40M	62.95G
PredRNN.V2	24.6M	708.0G	23.6M	2815.0G	23.8M	1223G	23.59M	279G	23.67M	42.63G	
Non-recurrent	TAU	37.6M	182.0G	15.0M	73.8G	44.7M	80.0G	12.22M	6.70G	9.55M	2.49G
	SimVP (w/o VQ)	28.8M	146.0G	12.2M	62.8G	15.6M	96.3G	12.76M	7.01G	7.84M	2.08G
	SimVP+SVQ	30.7M	178.0G	13.3M	110.0G	16.8M	156G	14.37M	16.8G	9.45M	3.72G

C. Additional experiments

C.1. Comparison of VQ methods using the same codebook size

To make a fair comparison, we extend Table 6 by setting the codebook size to the same value (1024) for all VQ methods. The VQ methods are evaluated from different aspects including downstream forecasting performance, codebook usage, and computational complexity. Additionally, we included a variant of residual VQ without stochastic sampling. In contrast to other VQ methods that rely on a single code, our SVQ generates multiple regression weights to merge several codes. To evaluate its perplexity, we first normalize the regression weights and then convert them into binary form using a threshold set at θ times the standard deviation, where θ serves as the threshold value. We utilize two thresholds (2 and 3) to obtain reasonable perplexity. The quantitative results are shown in Table 13. The convergence performance is shown in Figure 6, where SVQ quickly converges to the lowest prediction error and satisfactory utilization of the codebook. Residual VQ with stochastic sampling has the highest codebook usage (perplexity). However, its prediction MSE is worse than residual VQ without stochastic sampling. This demonstrates that codebook usage does not guarantee better downstream performance. SVQ generally outperforms the other VQ methods in computational efficiency, due to the simplified approximation described in Section 3.1.

Table 13. Quantitative comparison of VQ methods with the same codebook size (1024) on WeatherBench-S temperature dataset.

Vector quantization method	Prediction MSE↓	Perplexity↑	FLOPS↓	Inference FPS↑	Training time per epoch(min)↓
VQ	1.8544	51.95	7.207G	21.1	7.11
Residual VQ	1.2004	142.47	8.616G	7.7	13.25
Residual VQ (Stochastic)	1.8882	817.91	8.616G	8.1	17.27
Grouped Residual VQ	1.1737	132.57	8.616G	4.8	19.98
Multi-headed VQ	1.2113	16.36	8.717G	6.2	13.15
SVQ (freeze)	1.0393	335.72($\theta=3$)/438.39($\theta=2$)	8.037G	24.6	7.27
SVQ (Learnable)	1.0403	246.44($\theta=3$)/331.41($\theta=2$)	8.037G	24.9	7.30

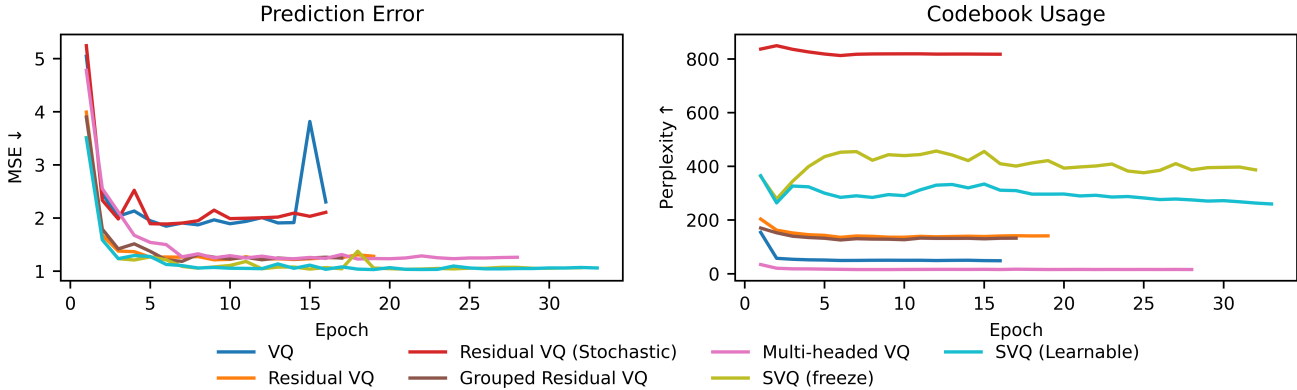


Figure 6. Prediction error and codebook usage of different VQ methods during the training process. All methods adopt the same codebook size (1024) and are earlystopped with a patience of 10 on WeatherBench-S temperature dataset. For simplicity, the perplexity of SVQ is averaged on different θ .

C.2. Position of quantization module

To illustrate how the position of quantization module affects representation learning, we consider two designs as shown in Figure 7. In our main draft, we adopt design (a) where quantization is performed before the translator. In this section, we also experimented with design (b) where quantization is performed after the translator. Interestingly, we found that the classic VQ method experiences significant divergence and codebook collapse issues under the latter design. Figure 8 illustrates the extreme instability of the classic VQ method during the training process when quantization is placed after the translator. We hypothesize that this instability is partly caused by non-differentiability of straight through estimator and the presence of diverse patterns. In contrast, our SVQ module never encounters such issues and remains highly stable throughout training.

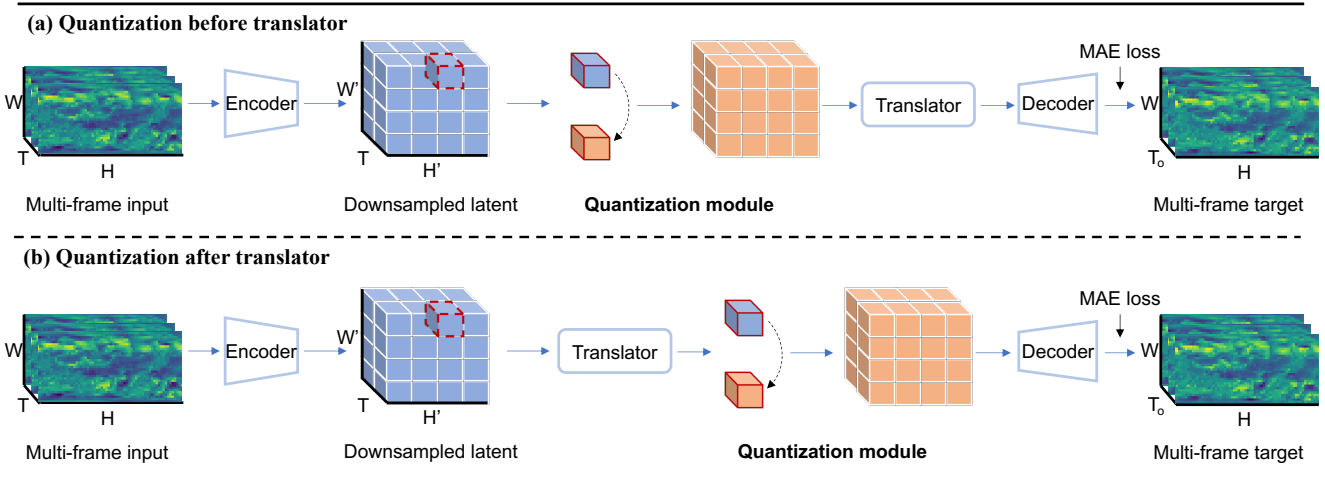


Figure 7. Comparison between two designs of quantization module with different positions: (a) before translator, and (b) after translator.

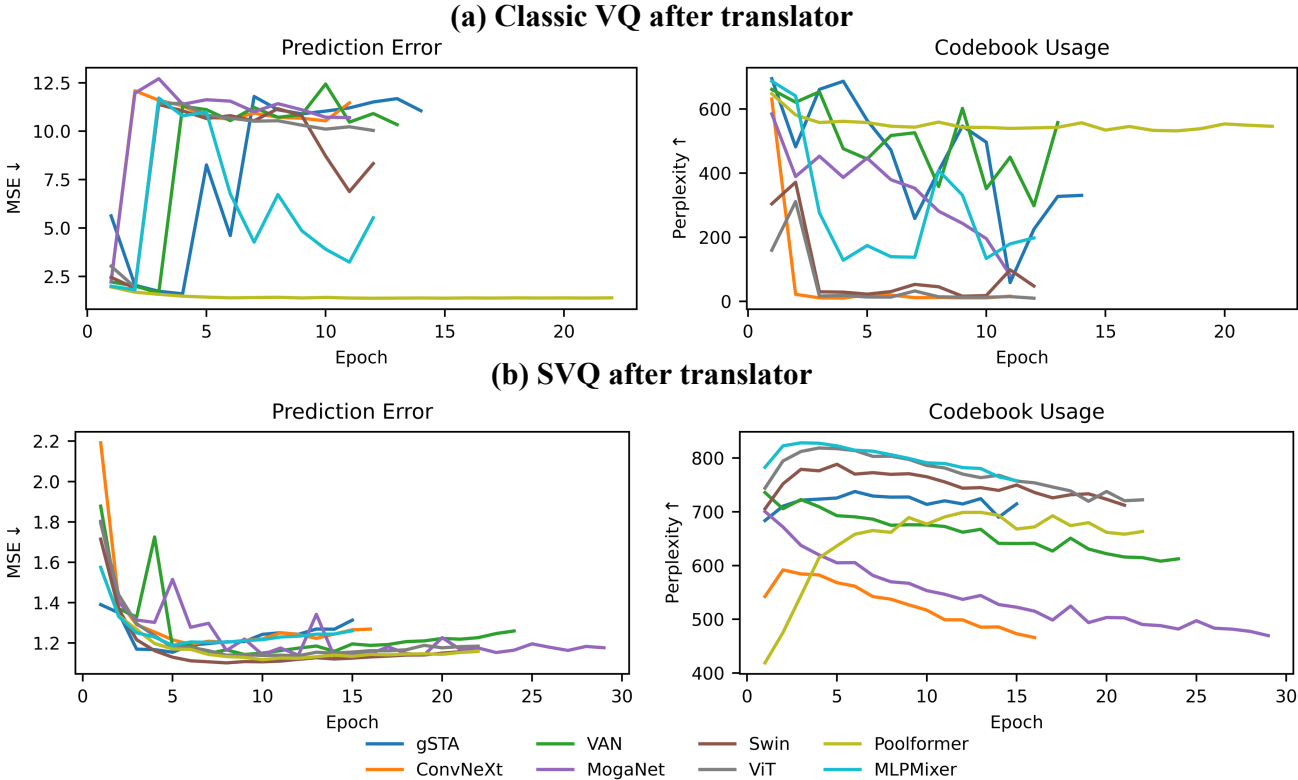


Figure 8. Comparison of SVQ and classic VQ when placed after translator. All methods adopt the same codebook size (1024) and are earlystopped with a patience of 10 on WeatherBench-S temperature dataset. For simplicity, the perplexity of SVQ is averaged on different θ .

C.3. Ablation of frozen module

The SVQ module consists of a two-layer MLP and a large codebook. The MLP can be seen as a projection from the input vector to the regression weights. In Section 5.3, we have already examined the impact of freezing the codebook on forecasting performance. To further investigate the effect of freezing the two-layer MLP, we conducted an ablation study in this section. The results, presented in Table 14, show that freezing the codebook only has a slight impact on forecasting performance, while freezing the MLP significantly impairs the performance.

Table 14. Ablation of frozen modules on WeatherBench-S temperature dataset.

Frozen module	None (All learnable)	Codebook	Two-layer MLP projection	Both
MSE	1.0182	1.0230	1.0602	1.0928
MAE	0.6109	0.6131	0.6194	0.6387

D. Additional qualitative results

D.1. Forecasting samples

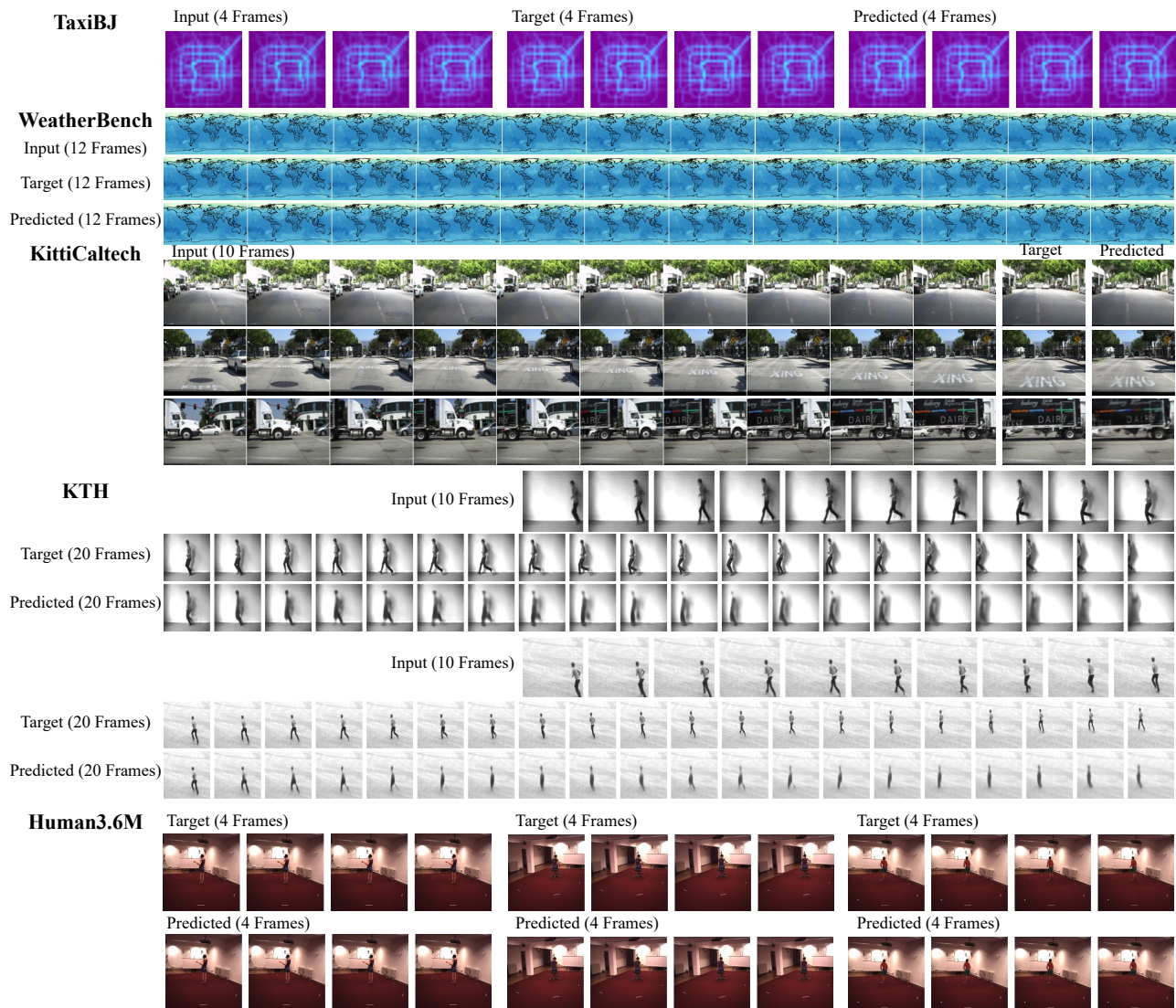


Figure 9. Forecasting samples of SimVP+SVQ model on the test set of TaxiBJ (32×32), WeatherBench (64×32), KittiCaltech (160×128), KTH (128×128), and Human3.6M (256×256). Zoom in for details. Our model produces accurate predicted frames for different tasks.

D.2. Effect of SVQ on latent representation

In Figure 5, we investigated the impact of SVQ on the sparsity of regression weights. To further investigate its effect on the latent representation, we compare the distribution of tensors before and after applying SVQ. We transform the tensors into normalized vectors and estimate their density distributions. As depicted in Figure 10, the representation after SVQ demonstrates a more compact distribution, indicating improved robustness to noise. Based on the results, we hypothesize that SVQ can enhance forecasting performance by effectively handling noise in the data.

Figures 11, 12, 13, 14, and 15 present the comparison of latent feature maps before and after applying SVQ. These figures illustrate that the difference between foreground and background in the feature maps increases after SVQ. For example, in the KittiCaltech dataset, a clear distinction is observed between road conditions and sky (11). In the WeatherBench-S temperature dataset, distinctive regions are identified between high and low latitudes (12). These observations suggest that SVQ helps in enhancing the discriminative power of the latent representations, leading to improved downstream forecasting performance.

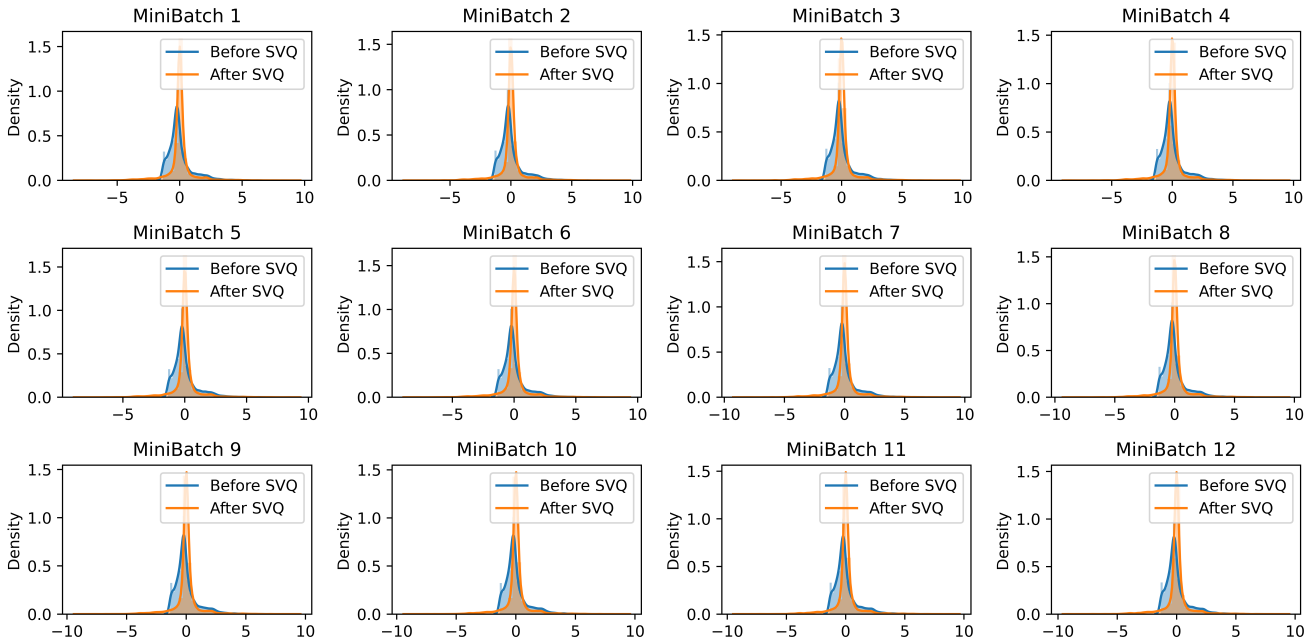


Figure 10. Distribution of latent vector on WeatherBench-S temperature dataset.

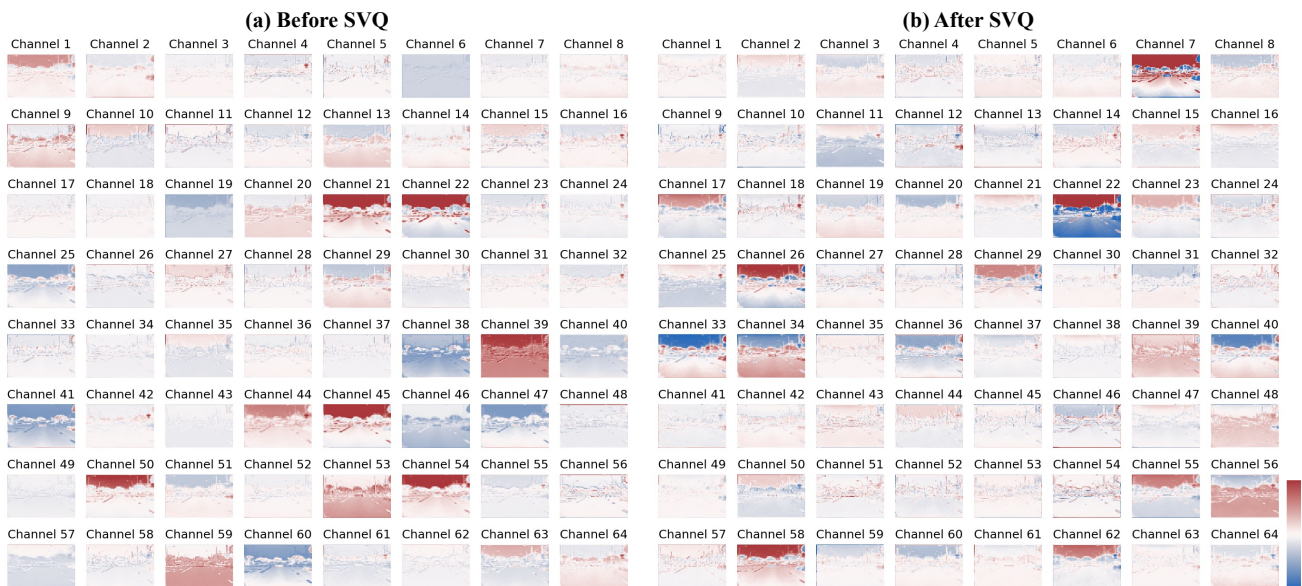


Figure 11. Latent feature map on the KittiCaltech dataset: (a) feature map before SVQ, and (b) feature map after SVQ.

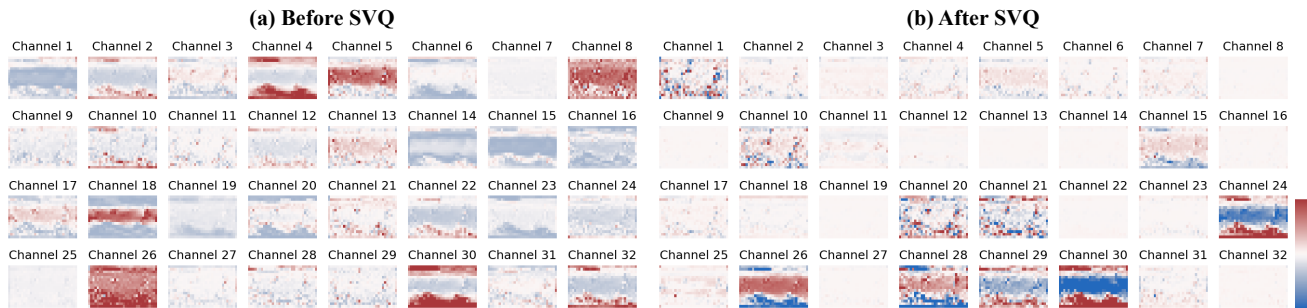


Figure 12. Latent feature map on the WeatherBench-S temperature dataset: (a) feature map before SVQ, and (b) feature map after SVQ.

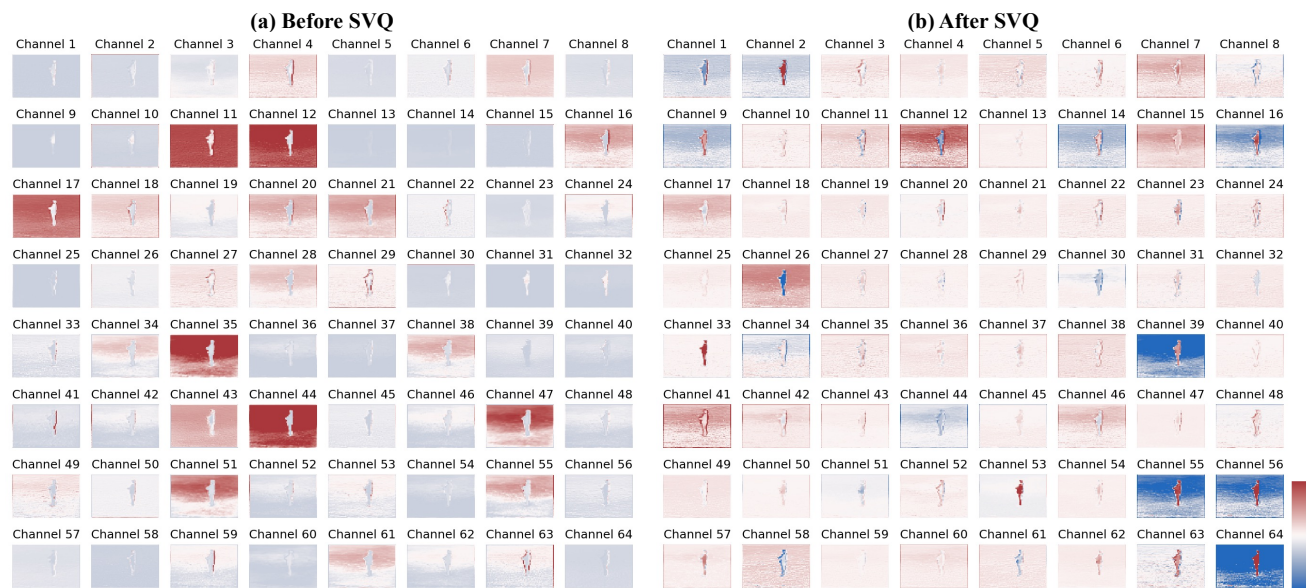


Figure 13. Latent feature map on the KTH dataset: (a) feature map before SVQ, and (b) feature map after SVQ.

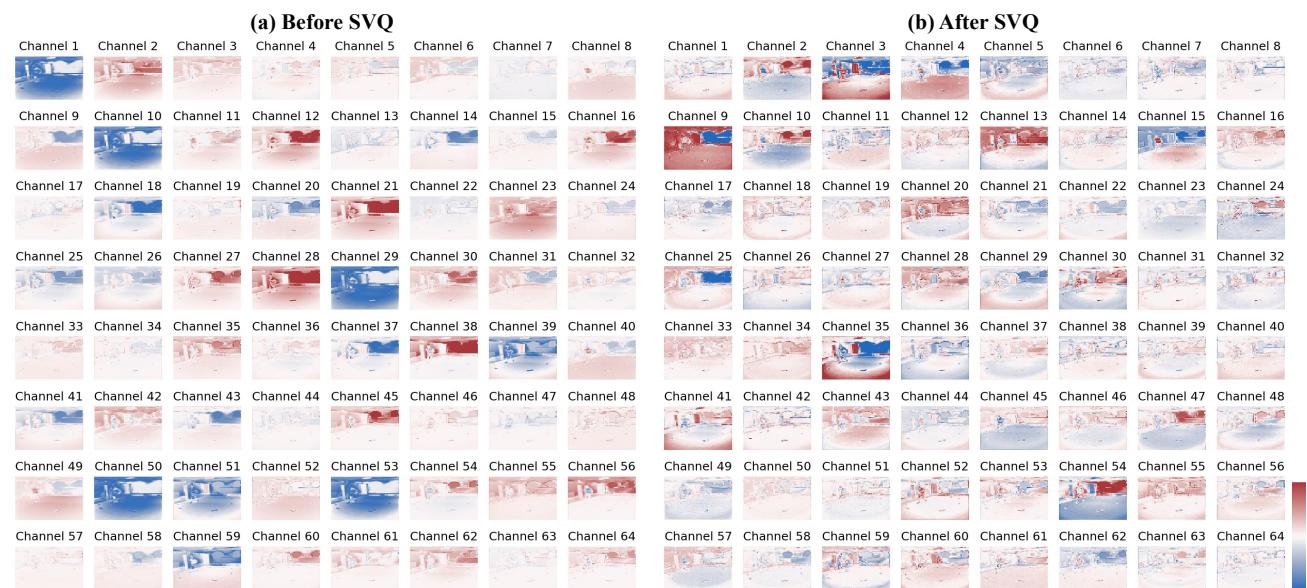


Figure 14. Latent feature map on the Human3.6M dataset: (a) feature map before SVQ, and (b) feature map after SVQ.

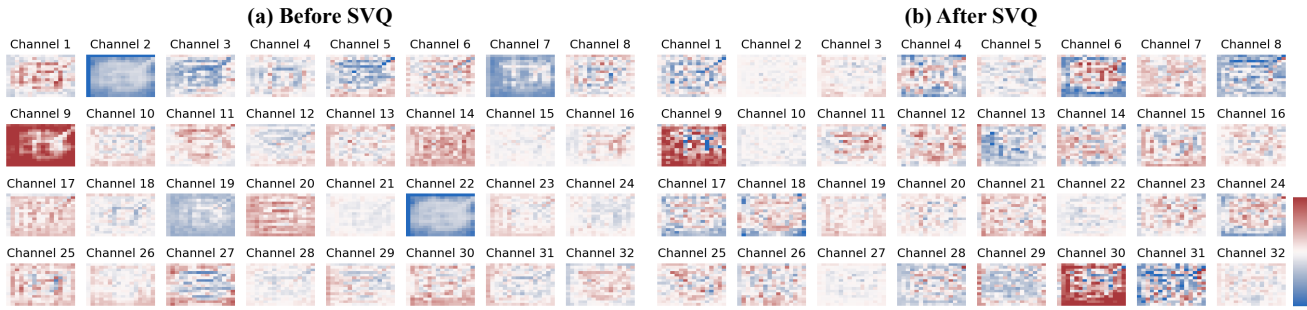


Figure 15. Latent feature map on the TaxiBJ dataset: (a) feature map before SVQ, and (b) feature map after SVQ.

References

- [1] Huiwen Chang, Han Zhang, Lu Jiang, Ce Liu, and William T. Freeman. Maskgit: Masked generative image transformer. In *IEEE/CVF Conference on Computer Vision and Pattern Recognition, CVPR 2022, New Orleans, LA, USA, June 18-24, 2022*, pages 11305–11315. IEEE, 2022. [1](#), [7](#)
- [2] Zheng Chang, Xinfeng Zhang, Shanshe Wang, Siwei Ma, Yan Ye, Xiang Xinguang, and Wen Gao. MAU: A motion-aware unit for video prediction and beyond. In *Advances in Neural Information Processing Systems 34: Annual Conference on Neural Information Processing Systems 2021, NeurIPS 2021, December 6-14, 2021, virtual*, pages 26950–26962, 2021. [5](#), [6](#), [7](#)
- [3] Ting Chen, Simon Kornblith, Mohammad Norouzi, and Geoffrey E. Hinton. A simple framework for contrastive learning of visual representations. In *Proceedings of the 37th International Conference on Machine Learning, ICML 2020, 13-18 July 2020, Virtual Event*, pages 1597–1607. PMLR, 2020. [1](#)
- [4] Chung-Cheng Chiu, James Qin, Yu Zhang, Jiahui Yu, and Yonghui Wu. Self-supervised learning with random-projection quantizer for speech recognition. In *International Conference on Machine Learning, 2022*. [2](#)
- [5] Piotr Dollár, Christian Wojek, Bernt Schiele, and Pietro Perona. Pedestrian detection: A benchmark. In *2009 IEEE Computer Society Conference on Computer Vision and Pattern Recognition (CVPR 2009), 20-25 June 2009, Miami, Florida, USA*, pages 304–311. IEEE Computer Society, 2009. [4](#)
- [6] Alexey Dosovitskiy, Lucas Beyer, Alexander Kolesnikov, Dirk Weissenborn, Xiaohua Zhai, Thomas Unterthiner, Mostafa Dehghani, Matthias Minderer, Georg Heigold, Sylvain Gelly, Jakob Uszkoreit, and Neil Houlsby. An image is worth 16x16 words: Transformers for image recognition at scale. In *9th International Conference on Learning Representations, ICLR 2021, Virtual Event, Austria, May 3-7, 2021*. OpenReview.net, 2021. [5](#)
- [7] Patrick Esser, Robin Rombach, and Björn Ommer. Taming transformers for high-resolution image synthesis. In *IEEE Conference on Computer Vision and Pattern Recognition, CVPR 2021, virtual, June 19-25, 2021*, pages 12873–12883. Computer Vision Foundation / IEEE, 2021. [2](#), [7](#)
- [8] Zhangyang Gao, Cheng Tan, Lirong Wu, and Stan Z. Li. Simvp: Simpler yet better video prediction. In *IEEE/CVF Conference on Computer Vision and Pattern Recognition, CVPR 2022, New Orleans, LA, USA, June 18-24, 2022*, pages 3160–3170. IEEE, 2022. [1](#), [2](#), [3](#), [5](#), [6](#), [7](#)
- [9] Andreas Geiger, Philip Lenz, Christoph Stiller, and Raquel Urtasun. Vision meets robotics: The KITTI dataset. *Int. J. Robotics Res.*, 32(11):1231–1237, 2013. [4](#)
- [10] Karol Gregor and Yann LeCun. Learning fast approximations of sparse coding. In *Proceedings of the 27th International Conference on Machine Learning (ICML-10), June 21-24, 2010, Haifa, Israel*, pages 399–406. Omnipress, 2010. [2](#)
- [11] Vincent Le Guen and Nicolas Thome. Disentangling physical dynamics from unknown factors for unsupervised video prediction. In *2020 IEEE/CVF Conference on Computer Vision and Pattern Recognition, CVPR 2020, Seattle, WA, USA, June 13-19, 2020*, pages 11471–11481. Computer Vision Foundation / IEEE, 2020. [5](#), [6](#), [7](#)
- [12] Meng-Hao Guo, Cheng-Ze Lu, Zheng-Ning Liu, Ming-Ming Cheng, and Shi-Min Hu. Visual attention network. *Comput. Vis. Media*, 9(4):733–752, 2023. [5](#)
- [13] Xiaotao Hu, Zhewei Huang, Ailin Huang, Jun Xu, and Shuchang Zhou. A dynamic multi-scale voxel flow network for video prediction. In *IEEE/CVF Conference on Computer Vision and Pattern Recognition, CVPR 2023, Vancouver, BC, Canada, June 17-24, 2023*, pages 6121–6131. IEEE, 2023. [5](#), [6](#)
- [14] Catalin Ionescu, Dragos Papava, Vlad Olaru, and Cristian Sminchisescu. Human3.6m: Large scale datasets and predictive methods for 3d human sensing in natural environments. *IEEE Trans. Pattern Anal. Mach. Intell.*, 36(7):1325–1339, 2014. [4](#)
- [15] Kunchang Li, Yali Wang, Junhao Zhang, Peng Gao, Guanglu Song, Yu Liu, Hongsheng Li, and Yu Qiao. Uniformer: Unifying convolution and self-attention for visual recognition. *IEEE Trans. Pattern Anal. Mach. Intell.*, 45(10):12581–12600, 2023. [5](#)
- [16] Siyuan Li, Zedong Wang, Zicheng Liu, Cheng Tan, Haitao Lin, Di Wu, Zhiyuan Chen, Jiangbin Zheng, and Stan Z. Li. Efficient multi-order gated aggregation network. *CoRR*, abs/2211.03295, 2022. [5](#)
- [17] Ze Liu, Yutong Lin, Yue Cao, Han Hu, Yixuan Wei, Zheng Zhang, Stephen Lin, and Baining Guo. Swin transformer: Hierarchical vision transformer using shifted windows. In *2021 IEEE/CVF International Conference on Computer Vision, ICCV 2021, Montreal, QC, Canada, October 10-17, 2021*, pages 9992–10002. IEEE, 2021. [5](#)
- [18] Zhuang Liu, Hanzi Mao, Chao-Yuan Wu, Christoph Feichtenhofer, Trevor Darrell, and Saining Xie. A convnet for the 2020s. In *IEEE/CVF Conference on Computer Vision and Pattern Recognition, CVPR 2022, New Orleans, LA, USA, June 18-24, 2022*, pages 11966–11976. IEEE, 2022. [5](#)
- [19] Ze Liu, Jia Ning, Yue Cao, Yixuan Wei, Zheng Zhang, Stephen Lin, and Han Hu. Video swin transformer. In *IEEE/CVF Conference on Computer Vision and Pattern Recognition, CVPR 2022, New Orleans, LA, USA, June 18-24, 2022*, pages 3192–3201. IEEE, 2022. [1](#)
- [20] William Lotter, Gabriel Kreiman, and David D. Cox. Deep predictive coding networks for video prediction and unsupervised learning. In *5th International Conference on Learning Representations, ICLR 2017, Toulon, France, April 24-26, 2017, Conference Track Proceedings*. OpenReview.net, 2017. [5](#), [6](#), [7](#)
- [21] Rayhane Mama, Marc S. Tyndel, Hashiam Kadhim, Cole Clifford, and Ragavan Thurairatnam. NWT: towards natural audio-to-video generation with representation learning. *CoRR*, abs/2106.04283, 2021. [2](#), [7](#)

- [22] Rayhane Mama, Marc S. Tyndel, Hashiam Kadhim, Cole Clifford, and Ragavan Thurairatnam. NWT: towards natural audio-to-video generation with representation learning. *CoRR*, abs/2106.04283, 2021. [2](#), [7](#)
- [23] Yongming Rao, Wenliang Zhao, Yansong Tang, Jie Zhou, Ser-Nam Lim, and Jiwen Lu. Hornet: Efficient high-order spatial interactions with recursive gated convolutions. In *NeurIPS*, 2022. [5](#)
- [24] Stephan Rasp, Peter D Dueben, Sebastian Scher, Jonathan A Weyn, Soukayna Mouatadid, and Nils Thuerey. Weatherbench: a benchmark data set for data-driven weather forecasting. *Journal of Advances in Modeling Earth Systems*, 12(11):e2020MS002203, 2020. [4](#)
- [25] Christian Schüldt, Ivan Laptev, and Barbara Caputo. Recognizing human actions: A local SVM approach. In *17th International Conference on Pattern Recognition, ICPR 2004, Cambridge, UK, August 23-26, 2004*, pages 32–36. IEEE Computer Society, 2004. [4](#)
- [26] Xingjian SHI, Hourong Chen, Hao Wang, Dit-Yan Yeung, Wai-kin Wong, and Wang-chun WOO. Convolutional lstm network: A machine learning approach for precipitation nowcasting. In *Advances in Neural Information Processing Systems*. Curran Associates, Inc., 2015. [1](#), [2](#), [5](#), [6](#), [7](#)
- [27] Cheng Tan, Zhangyang Gao, and Stan Z. Li. Simvp: Towards simple yet powerful spatiotemporal predictive learning. *CoRR*, abs/2211.12509, 2022. [1](#), [2](#), [5](#)
- [28] Cheng Tan, Zhangyang Gao, Lirong Wu, Yongjie Xu, Jun Xia, Siyuan Li, and Stan Z. Li. Temporal attention unit: Towards efficient spatiotemporal predictive learning. In *IEEE/CVF Conference on Computer Vision and Pattern Recognition, CVPR 2023, Vancouver, BC, Canada, June 17-24, 2023*, pages 18770–18782. IEEE, 2023. [1](#), [2](#), [5](#), [6](#), [7](#)
- [29] Cheng Tan, Siyuan Li, Zhangyang Gao, Wenfei Guan, Zedong Wang, Zicheng Liu, Lirong Wu, and Stan Z. Li. Openstl: A comprehensive benchmark of spatio-temporal predictive learning. *CoRR*, abs/2306.11249, 2023. [2](#), [4](#), [5](#)
- [30] Ilya O. Tolstikhin, Neil Houlsby, Alexander Kolesnikov, Lucas Beyer, Xiaohua Zhai, Thomas Unterthiner, Jessica Yung, Andreas Steiner, Daniel Keysers, Jakob Uszkoreit, Mario Lucic, and Alexey Dosovitskiy. Mlp-mixer: An all-mlp architecture for vision. In *Advances in Neural Information Processing Systems 34: Annual Conference on Neural Information Processing Systems 2021, NeurIPS 2021, December 6-14, 2021, virtual*, pages 24261–24272, 2021. [5](#)
- [31] Asher Trockman and J. Zico Kolter. Patches are all you need? *Trans. Mach. Learn. Res.*, 2023, 2023. [5](#)
- [32] Aäron van den Oord, Oriol Vinyals, and Koray Kavukcuoglu. Neural discrete representation learning. In *Advances in Neural Information Processing Systems 30: Annual Conference on Neural Information Processing Systems 2017, December 4-9, 2017, Long Beach, CA, USA*, pages 6306–6315, 2017. [2](#), [7](#)
- [33] Yunbo Wang, Mingsheng Long, Jianmin Wang, Zhifeng Gao, and Philip S. Yu. Predrnn: Recurrent neural networks for predictive learning using spatiotemporal lstms. In *Advances in Neural Information Processing Systems 30: Annual Conference on Neural Information Processing Systems 2017, December 4-9, 2017, Long Beach, CA, USA*, pages 879–888, 2017. [1](#), [2](#), [5](#), [6](#), [7](#)
- [34] Yunbo Wang, Zhifeng Gao, Mingsheng Long, Jianmin Wang, and Philip S. Yu. Predrnn++: Towards A resolution of the deep-in-time dilemma in spatiotemporal predictive learning. In *Proceedings of the 35th International Conference on Machine Learning, ICML 2018, Stockholmsmässan, Stockholm, Sweden, July 10-15, 2018*, pages 5110–5119. PMLR, 2018. [2](#), [5](#), [6](#), [7](#)
- [35] Yunbo Wang, Lu Jiang, Ming-Hsuan Yang, Li-Jia Li, Mingsheng Long, and Li Fei-Fei. Eidetic 3d LSTM: A model for video prediction and beyond. In *7th International Conference on Learning Representations, ICLR 2019, New Orleans, LA, USA, May 6-9, 2019*. OpenReview.net, 2019. [1](#), [5](#), [6](#), [7](#)
- [36] Yunbo Wang, Jianjin Zhang, Hongyu Zhu, Mingsheng Long, Jianmin Wang, and Philip S. Yu. Memory in memory: A predictive neural network for learning higher-order non-stationarity from spatiotemporal dynamics. In *IEEE Conference on Computer Vision and Pattern Recognition, CVPR 2019, Long Beach, CA, USA, June 16-20, 2019*, pages 9154–9162. Computer Vision Foundation / IEEE, 2019. [5](#), [6](#), [7](#)
- [37] Yunbo Wang, Haixu Wu, Jianjin Zhang, Zhifeng Gao, Jianmin Wang, Philip Yu, and Mingsheng Long. Predrnn: A recurrent neural network for spatiotemporal predictive learning. *IEEE Transactions on Pattern Analysis and Machine Intelligence*, pages 1–1, 2022. [2](#), [5](#), [6](#), [7](#)
- [38] Zhou Wang, Alan C. Bovik, Hamid R. Sheikh, and Eero P. Simoncelli. Image quality assessment: from error visibility to structural similarity. *IEEE Trans. Image Process.*, 13(4):600–612, 2004. [4](#)
- [39] Pan Xiao, Peijie Qiu, and Aristeidis Sotiras. SC-VAE: sparse coding-based variational autoencoder. *CoRR*, abs/2303.16666, 2023. [2](#), [7](#)
- [40] Ziru Xu, Yunbo Wang, Mingsheng Long, and Jianmin Wang. Predcnn: Predictive learning with cascade convolutions. In *Proceedings of the Twenty-Seventh International Joint Conference on Artificial Intelligence, IJCAI 2018, July 13-19, 2018, Stockholm, Sweden*, pages 2940–2947. ijcai.org, 2018. [1](#)
- [41] Dongchao Yang, Songxiang Liu, Rongjie Huang, Jinchuan Tian, Chao Weng, and Yuexian Zou. Hifi-codec: Group-residual vector quantization for high fidelity audio codec. *CoRR*, abs/2305.02765, 2023. [2](#), [7](#)
- [42] Lijun Yu, José Lezama, Nitesh Bharadwaj Gundavarapu, Luca Versari, Kihyuk Sohn, David Minnen, Yong Cheng, Agrim Gupta, Xiuye Gu, Alexander G. Hauptmann, Boqing Gong, Ming-Hsuan Yang, Irfan Essa, David A. Ross, and Lu Jiang. Language model beats diffusion - tokenizer is key to visual generation. *CoRR*, abs/2310.05737, 2023. [2](#), [7](#)
- [43] Weihao Yu, Mi Luo, Pan Zhou, Chenyang Si, Yichen Zhou, Xinchao Wang, Jiashi Feng, and Shuicheng Yan. Metaformer is actually what you need for vision. In *IEEE/CVF Conference on Computer Vision and Pattern Recognition, CVPR 2022, New Orleans, LA, USA, June 18-24, 2022*, pages 10809–10819. IEEE, 2022. [4](#), [5](#)

- [44] Weihao Yu, Mi Luo, Pan Zhou, Chenyang Si, Yichen Zhou, Xinchao Wang, Jiashi Feng, and Shuicheng Yan. Metaformer is actually what you need for vision. In *IEEE/CVF Conference on Computer Vision and Pattern Recognition, CVPR 2022, New Orleans, LA, USA, June 18-24, 2022*, pages 10809–10819. IEEE, 2022. 5
- [45] Neil Zeghidour, Alejandro Luebs, Ahmed Omran, Jan Skoglund, and Marco Tagliasacchi. Soundstream: An end-to-end neural audio codec. *IEEE ACM Trans. Audio Speech Lang. Process.*, 30:495–507, 2022. 2, 7
- [46] Junbo Zhang, Yu Zheng, and Dekang Qi. Deep spatio-temporal residual networks for citywide crowd flows prediction. In *Proceedings of the Thirty-First AAAI Conference on Artificial Intelligence, February 4-9, 2017, San Francisco, California, USA*, pages 1655–1661. AAAI Press, 2017. 4
- [47] Richard Zhang, Phillip Isola, Alexei A. Efros, Eli Shechtman, and Oliver Wang. The unreasonable effectiveness of deep features as a perceptual metric. In *2018 IEEE Conference on Computer Vision and Pattern Recognition, CVPR 2018, Salt Lake City, UT, USA, June 18-22, 2018*, pages 586–595. Computer Vision Foundation / IEEE Computer Society, 2018. 4